Supplementary Material

Simulation control images

As control experiments for particle bleed-through, we simulated a system where particles with different spectral emissions diffused freely within spatially separated compartments. Specifically, green-emitting particles were confined to a central circular region, whereas red-emitting particles were restricted to an annular region surrounding it (Figure S1, schematic). All particles underwent free diffusion with a diffusion coefficient of 10 μm²/s, and image acquisition was simulated using a raster scan at 10 μs/pixel. To simulate spectral bleeding, green particles were assigned emission rates at 10^6 cps in the green channel and 10^5 cps in the red channel (10% bleeding), while red particles emitted 10^6 cps in the red channel and 10^4 cps in the green channel (1% bleeding). Control datasets for each fluorophore were also simulated under identical acquisition conditions, allowing for the accurate estimation of the bleeding matrix.

The spatial separation between the two particle populations was introduced solely to facilitate visual assessment of the spectral unmixing performance. As shown in Figure S1, a detectable signal is observed in the red channel over the central circle, where only green particles are present, confirming red-channel contamination from the green population. In contrast, the 1% bleeding from red to green is less visually apparent, yet, as previously demonstrated and shown again in this simulation, even low levels of bleeding can significantly affect correlation-based analyses and must be corrected. Using the control simulations, we derived the correction matrix p, defined in this case as:

$$p = \begin{bmatrix} 10 & 0.1 \\ 1 & 10 \end{bmatrix}.$$

Upon applying the spectral unmixing procedure to the simulated concentric-circle images, the corrected (unmixed) images are shown in Figure S1. Notably, the spurious signal observed in the red channel at the center of the image, originating from green-to-red bleeding, is substantially reduced, indicating effective suppression of the spurious signal. Although the visual inspection of the unmixed images suggests

successful correction, a more rigorous validation requires quantitative correlation analysis (Figure 4 in the main text).

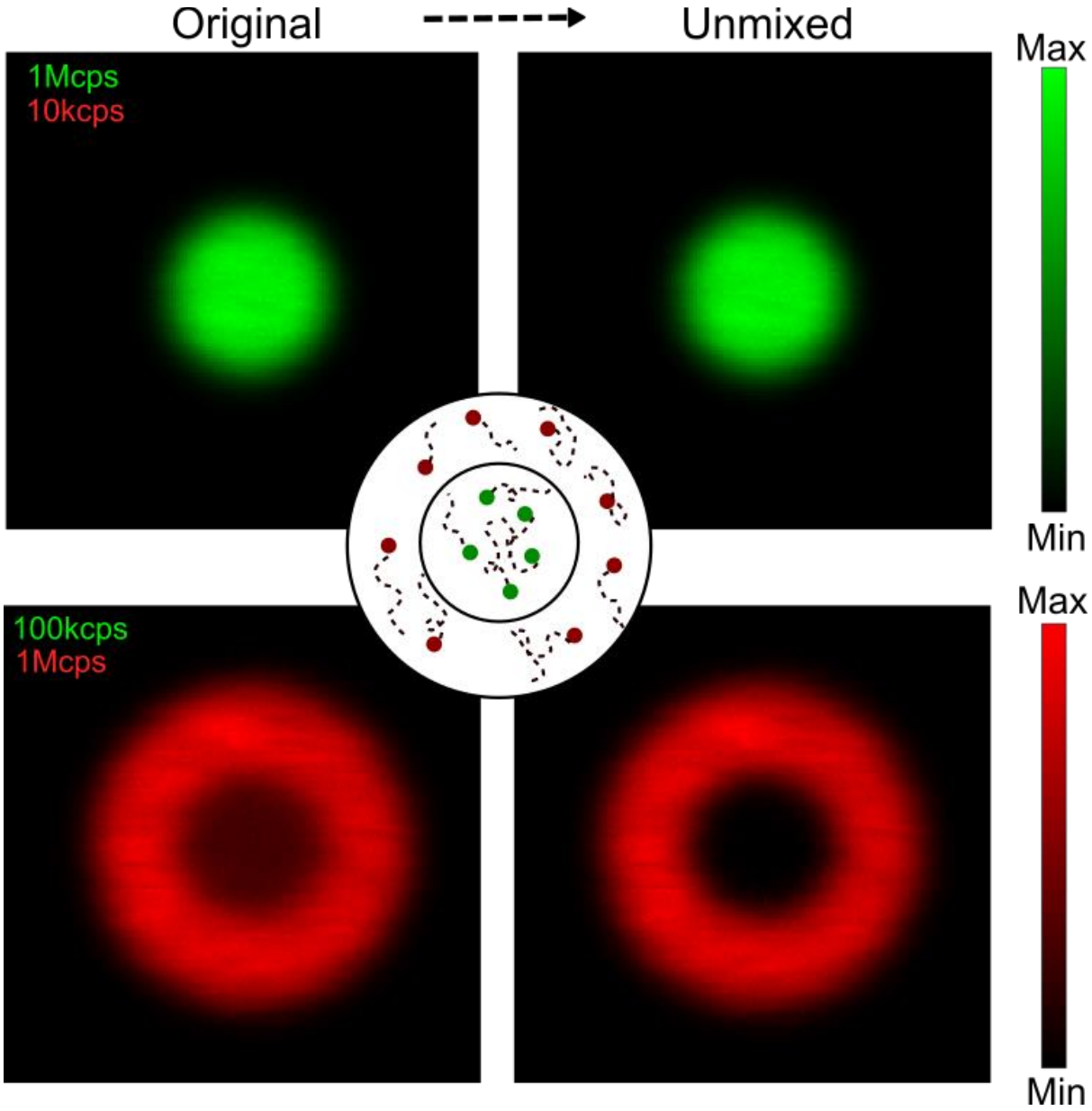

Figure S1: Spectral bleeding correction in control simulations. Simulated raster-scan images of two spatially separated particle populations: green-emitting particles are confined to the central circle, and red-emitting particles occupy the surrounding ring. The raw images (left column) exhibit spectral bleeding, particularly from green into the red detection channel, as evidenced by a signal detected in the red channel over the central region where no red particles are present. In contrast, the 1% bleed-through from red to green is less visually apparent but still impacts downstream analysis. Spectral demixing (right column) restores the correct particle distributions, demonstrating effective removal of cross-channel spectral bleeding.

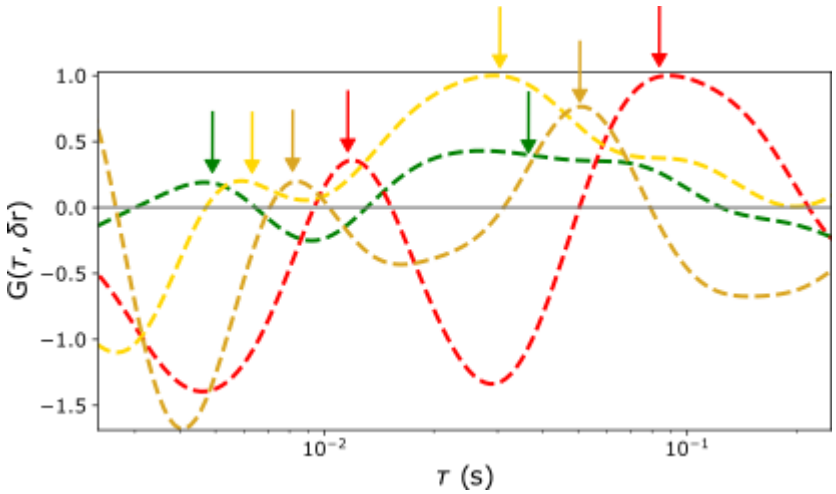

Figure S2: Complementary curve for Figure 6 in the main text*. pCF(16) is shown for pixels in the nucleus that correlate to pixels in the cytoplasm. RBM10-EGFP (green) and NS5-mCherry (red) are shown as well as the ccpCF curves, one correlating the green channel on the nucleus to the red channel on the cytoplasm (yellow) and the other one inverting the channels (olive). The peaks corresponding to the translocation times are pointed out.*

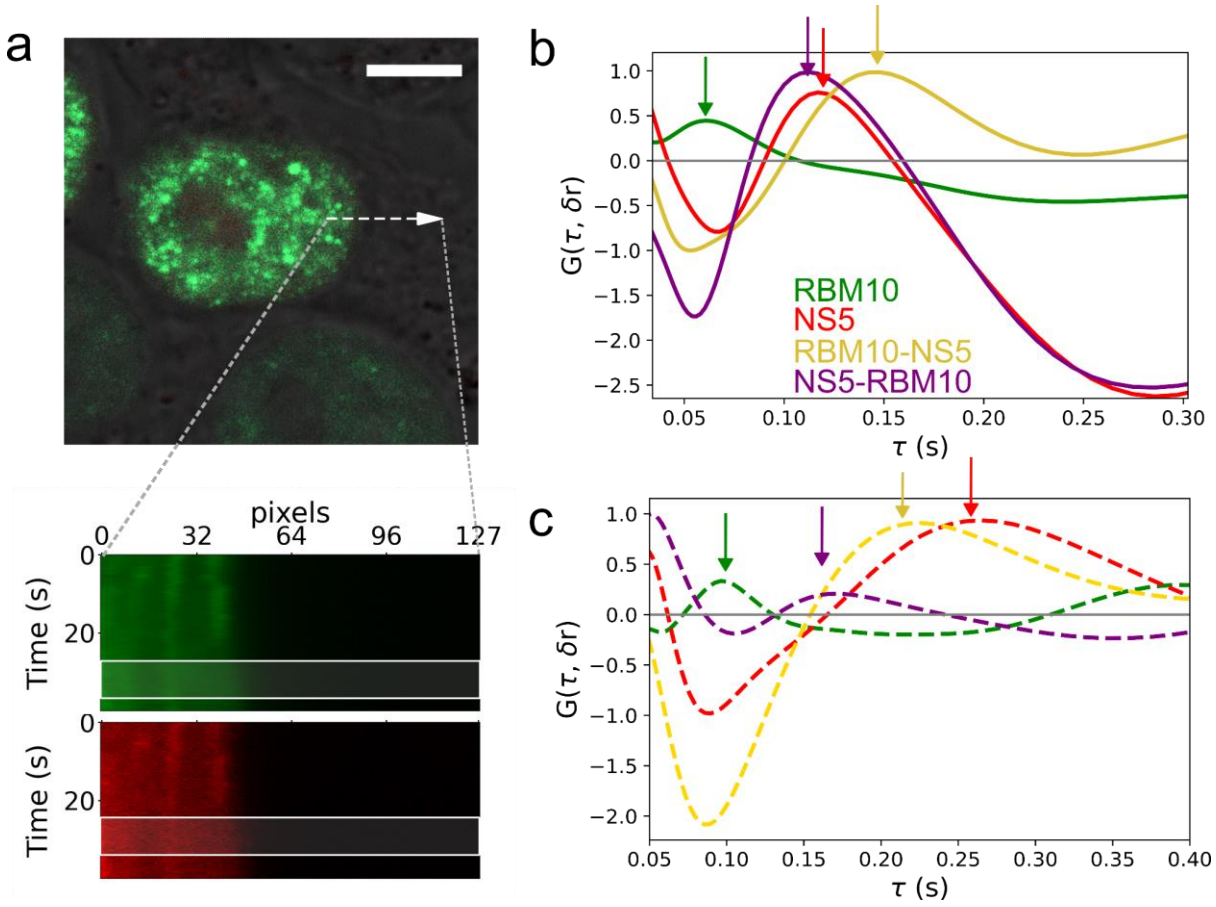

Figure S3: RBM10 and NS5 exhibit cross-correlation in cells transfected with poly (I:C). *(a) Dual-color line scanning experiments were performed across the nuclear membrane of cells transfected with poly (I:C) cotransfected with RBM10-EGFP and mCherry-NS5 (the scale bar represents 5 µm). This allowed simultaneous measurement of the transport time for both proteins. From a total of 200,000 acquired lines, a subset of 50,000 lines (white box) was selected for analysis. By correlating pixels in the cytoplasm, close to the membrane, with those in the nucleus (entry direction), the translocation times for both proteins were determined. The pCF(16) is shown for pixels in the cytoplasm correlated with pixels in the nucleus (b) and for the nucleus correlated with pixels in the cytoplasm (c). The pCF curves for RBM10-EGFP (green) and mCherry-NS5 (red) are shown, along with the ccpCF curves: one correlating the green channel with the red channel (purple), and the other one inverting the channels (yellow). Arrows indicate the peaks corresponding to the translocation times.*

Cross-correlation controls

As control experiments, we conducted ccpCF analysis on cells cotransfected with RBM10-EGFP and mCherry and cells cotransfected with EGFP and mCherry-NS5. Due to the spectral bleeding, even though no cross-correlation is expected, about 40% of the cells studied present positive ccpCF. By performing the deximing of the signals, these dropped below 20% while the same process kept the RBM10-NS5 ccpCF unchanged (Figure S4).

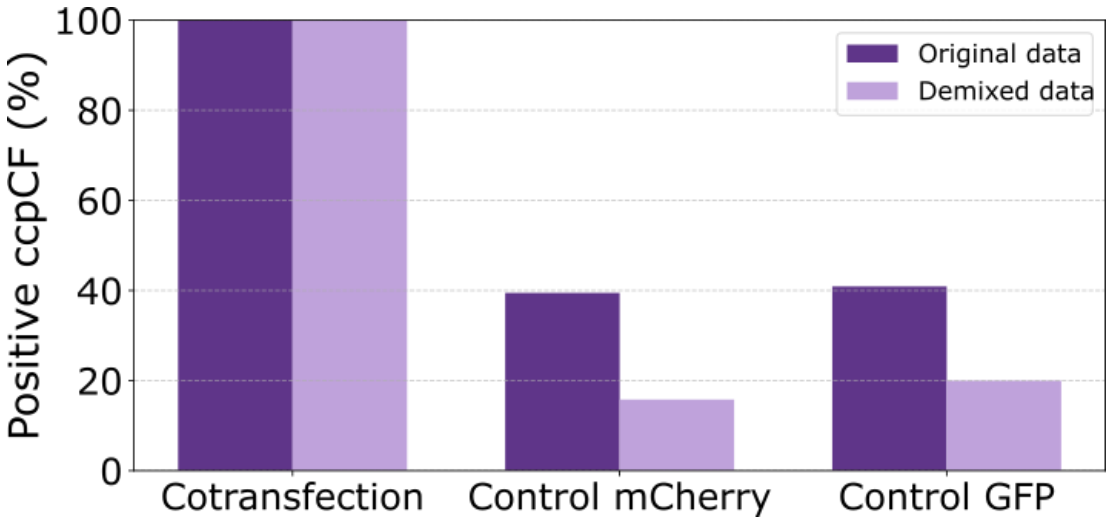

Figure S4: The demixing algorithm eliminates artificial cross-correlation. *ccpCF results yielded positive ccpCF in all cells cotransfected with RBM10-EGFP and mCherry-NS5, whereas the control conditions using RBM10-EGFP cotransfected with mCherry (Control mCherry) and EGFP-C1 cotransfected with mCherry-NS5 (Control GFP) showed fewer than 20% positive ccpCF curves after demixing.*

EGFP control experiments

As a control, we performed pCF experiments on cells overexpressing EGFP-C1 both with or without poly (I:C) transfection. Nuclear entry and exit were analyzed by acquiring line scans

across the nuclear membrane (Figure S5 a). Subsequently, we performed pCF(16) analysis as applied for RBM10 (Figure S5 b) in both directions to obtain the entry and exit correlation delays for each cell (Figure S5 c for EGFP-C1 without poly (I:C) and Figure S5 d with poly (I:C)). The correlation times measured across 20 cells (D=2) for the condition EGFP-C1 without poly (I:C) and 11 cells (D=2) for EGFP-C1 with poly (I:C) were statistically indistinguishable (Figure S5 e) for both nuclear entry and exit. These findings confirm that the results observed for RBM10-EGFP upon poly(I:C) treatment are attributable to RBM10 itself, as the fluorophore dynamic remains unaltered when expressed alone.

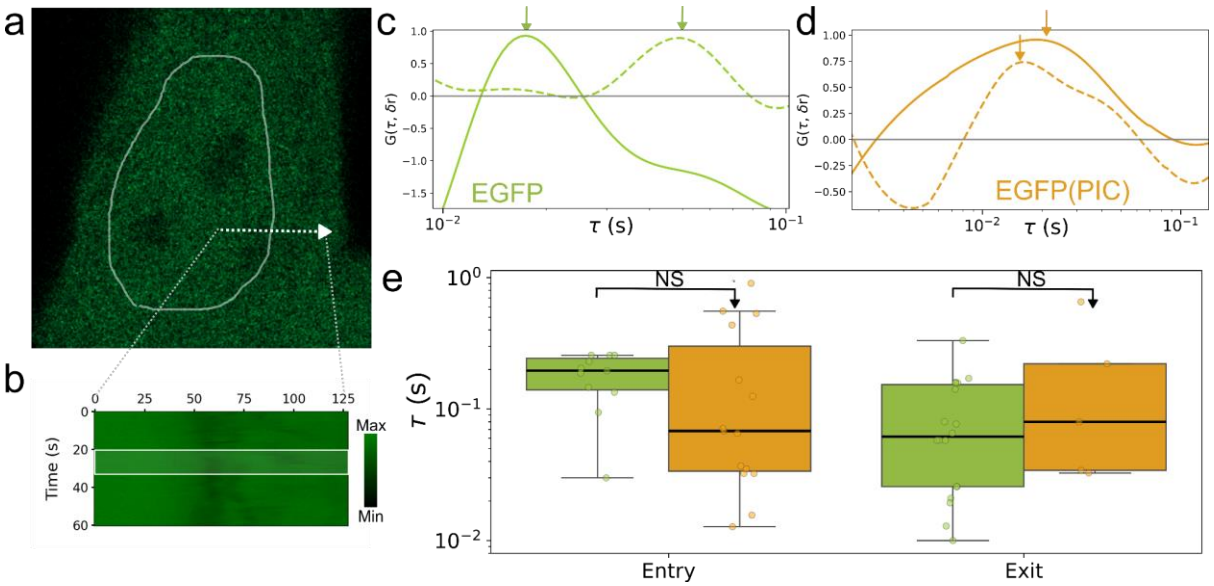

Figure S5: EGFP-C1 nuclear transport is unaffected by poly (I:C) transfection. Line scan experiments across the nuclear membrane were performed in cells transfected with EGFP-C1 (a). By correlating the intensity signal (b), we obtained the corresponding pCF(16) kymograms. By correlating pixels from one side of the membrane to the other, nuclear entry (dotted line) and exit (filled line) transport times were determined (c). The same analysis was performed over EGFP-C1 cells treated with poly (I:C). Comparison of transport times between the two conditions revealed no statistically significant differences in nuclear entry nor exit dynamics, confirming that poly(I:C) does not alter the transport properties of EGFP-C1 alone. (e).